Title

Climate sensitivity of spring snowpack in the Sierra Nevada

Journal

Journal of Geophysical Research-Earth Surface, 110(F4)

ISSN

0148-0227

Authors

Howat, Ian M

Tulaczyk, S

Publication Date

2005-12-01

Peer reviewed

Climate sensitivity of spring snowpack in the Sierra Nevada

Ian M. Howat and Slawek Tulaczyk

Department of Earth Sciences, University of California, Santa Cruz, California, USA

Received 21 June 2005; revised 26 September 2005; accepted 7 October 2005; published 8 December 2005.

[1] California's spring snowpack provides a critical water resource that may be greatly reduced by greenhouse warming. However, warming over the past half century has had little effect on total summer water discharge. The region's snowpack may therefore be less sensitive to temperature change than predicted by numerical models. In this study, 53 years of 1 April snow course measurements of snow-water equivalent (SWE) from the Sierra Nevada are used in a spatially distributed covariance model of SWE sensitivity to temperature and precipitation. This model is applied at a 2.5 arc min resolution using a multivariate parameter-surface interpolation scheme and Parameter-elevation Regressions on Independent Slopes (PRISM) climate grids. Total modeled SWE volume has a greater covariance to precipitation than to temperature. Increasing precipitation and temperature from 1950 to 2002 has led to an increase in SWE at high elevations and a loss at low elevations, resulting in little or no overall change in SWE volume. The covariance model predicts a 6–10% decrease in total SWE volume per °C. However, sensitivity is both highly dependent on concurrent change in precipitation and spatially variable, with the lower-elevation watersheds in the north being the most sensitive to warming. Overall, climate sensitivity is much less than that predicted by numerical models. This difference may result from inadequate treatment of elevation and precipitation in climate models.

Citation: Howat, I. M., and S. Tulaczyk (2005), Climate sensitivity of spring snowpack in the Sierra Nevada, *J. Geophys. Res.*, *110*, F04021, doi:10.1029/2005JF000356.

1. Introduction

[2] Since most of the annual precipitation in California occurs during the winter, the summer discharge of its major rivers is supplied mostly by melting of winter snow accumulation at high elevations [*Serreze et al.*, 1999]. Therefore the impact of climate change on seasonal snow water volume could have far-reaching implications for regional hydrology [*California Energy Commission*, 2003]. Warming during the winter months would result in more rain, as opposed to snow, at lower elevations, decreasing summer water supply and increasing the recurrence and amplitude of winter and spring flood events [*Miller et al.*, 2003]. Since existing water resources are already committed within much of California, any decrease in summer river discharge will need to be mitigated with either reservoir construction or conservation policies [*California Department of Water Resources*, 1998]. Effective preparation and planning for a potential decrease in water supply would require high-confidence estimates of the near-future response of snowpack to greenhouse warming scenarios for individual drainages.

[3] Several studies have examined the potential effects of predicted greenhouse warming on Sierra Nevada's spring snowpack using a variety of physically based numerical climate and watershed models [*Kim*, 2001; *Kim et al.*, 2002; *Knowles and Cayan*, 2002; *Snyder et al.*, 2002, 2004]. These models suggest a high sensitivity of snowpack to temperature, ranging from a 60% to a nearly 100% reduction in mean 1 April snow-water equivalent (SWE) under a warming of 2°–4°C. However, despite an observed winter warming of up to 3°C over the last half of the twentieth century, measurements of spring SWE show little overall trend, and there has been little or no change in total summer river discharge [*Howat and Tulaczyk*, 2005; *Shelton and Fridirici*, 1997]. This is because significant decreases in spring snow-water equivalent have occurred at only the lowest elevations and may have been partially offset by a significant increase at higher elevations [*Howat and Tulaczyk*, 2005]. Although this may indicate a much lower sensitivity of snow water volume to temperature than suggested by numerical models, no detailed spatial analysis of the long-term observational record has been undertaken.

[4] The observational record needed for a long-term assessment of climate forcing on snow volume and distribution lies in historical snow course observations. Nearly a century of monthly snow course data exists for the Sierra Nevada, representing one of the longest and most spatially dense records of snow hydrology in the world (Figure 1). A single snow course measurement is the average of several point measurements, usually located in open, flat areas. This makes snow course measurements uncertain representations of the average snowpack for areas where surface conditions differ from those at the snow course site. However, the temporal variations are less sensitive to local factors, such

0148-0227/05/2005JF000356$09.00

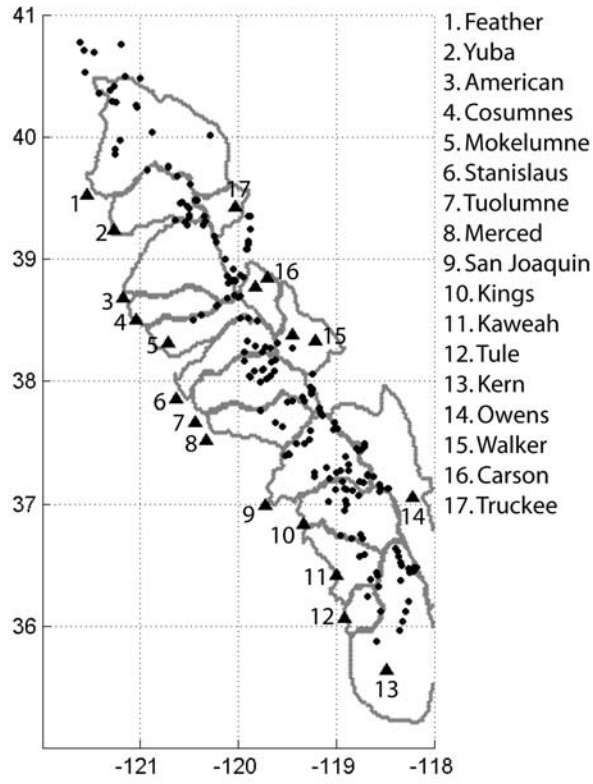

Figure 1. Map of Sierra Nevada snow courses (circles), watershed boundaries (gray lines), and river gauges (triangles) used in this study.

as changes in foliage or drift patterns, and are more sensitive to variations in climate [*Bohr and Aguado*, 2001]. Therefore, while historical snow course measurements may be poor predictors of snow volume for any given year, they provide a much more robust indication of climate-driven temporal variations and, consequently, the sensitivity of snowpack to climate forcing at a regional scale.

[5] The objective of this study is to determine the climate sensitivity of Sierra Nevada's 1 April SWE^3 on the basis of spatial-temporal analysis of observations between 1950 and 2002. We first reconstruct SWE^3 through interpolation of annual snow course measurements. Estimated SWE^3 distributions are then correlated to existing high-resolution maps of temperature and precipitation to produce a spatially distributed estimate of climate sensitivity. This sensitivity is assessed on both the regional and watershed scales and is compared to estimates produced by numerical models.

2. Data

[6] We use 1 April SWE measurements from 177 snow courses in the Sierra Nevada of California and western Nevada operated by the California Cooperative Snow Survey and distributed by the U.S. Department of Agriculture (see http://www.wcc.nrcs.usda.gov/snowcourse and the auxiliary material[1]) (Figure 1). A detailed description of the data collection and verification program is given by *Roos* [2003]. These stations are missing no more than five measurements from the period 1950–2002, with no more than two consecutive years missing. While some snow courses have records extending to the early 1900s, we use the period 1950–2002 because our analysis requires a temporally homogenous data set (i.e., the same group of stations must be used throughout the time period) and many more stations are available after 1950. Also, as stated above, this is the period of a strong winter warming trend. The April 1 date is chosen because it provides, by far, the largest data set and is, on regional average, closest to the date of maximum SWE.

[7] Gridded monthly mean temperature and total precipitation were obtained from 2.5 arc min resolution maps generated from the Parameter-elevation Regressions on Independent Slopes (PRISM) interpolation model (see http://www.ocs.orst.edu/prism). These data sets have undergone extensive validation and provide the highest-resolution gridded climate maps available [*Daly et al.*, 2000a].

[8] Total summer (April–September) full natural flow data for 17 major Sierra Nevada drainages (Figure 1) were obtained from the California Data Exchange Center (see http://cdec.water.ca.gov). Watershed boundaries used to compare estimated snow water volume with summer river discharge were obtained from the California Department of Water Resources (see http://wwwdwr.water.ca.gov).

3. Methods

3.1. Spatial Interpolation Model

[9] Comparative studies of interpolating snow measurements over large, topographically complex regions have found that surface detrending coupled with distance-weighted residual interpolation yields optimal results [*Carroll and Cressie*, 1997; *Daly et al.*, 2000b; *Erxleben et al.*, 2002; *Fassnacht et al.*, 2003; *Marquinez et al.*, 2003]. This method also has the advantage of being easily adapted over space and time through parameter fitting and yields estimate confidence intervals. Binary decision trees and neural networks have also been employed with success [*Balk and Elder*, 2000; *Erxleben et al.*, 2002]. However, these methods are not easily automated (e.g., regression tree "pruning" and neural classification); they are difficult to interpret physically, and their uncertainties are difficult to asses.

[10] We employ a multivariate parameter-surface modeling approach in which we assume the linear system

$$\hat{\mathrm{SWE}} = \boldsymbol{\beta} \cdot \mathbf{x} + \varepsilon, \tag{1}$$

where

$$\boldsymbol{\beta} = \begin{bmatrix} \beta_0 \\ \beta_1 \\ \vdots \\ \beta_{n \cdot p} \end{bmatrix},$$

$$\mathbf{x} = \begin{bmatrix} 1 & x_1^1 & \dots & x_n^p \end{bmatrix},$$

$\hat{\mathrm{SWE}}$ is the predicted snow-water equivalent, $\mathbf{x}$ and $\boldsymbol{\beta}$ are vectors of independent variables and empirical model parameters, respectively, and ε is the random model residual. Each vector contains $np + 1$ elements, where n is

[1] Auxiliary material is available at ftp://ftp.agu.org/apend/jf/2005JF000356.

the number of independent variables used in the model and p is the maximum order of the model. We include higher-order terms ($2 \ldots p$) because of the observed highly nonlinear relation between snow distribution and physiographic and climactic variables [*Aguado*, 1990]. The model residual ε is interpolated from the population of data points to the estimate location using anisotropic distance-weighted averaging:

$$\varepsilon = \frac{\sum_{x,y=1}^{n} \left[\varepsilon e^{-Dxi/\eta_x}, \varepsilon e^{-Dyi/\eta_y} \right]}{\sum_{x,y=1}^{n} \left[e^{-Dxi/\eta_x}, e^{-Dyi/\eta_y} \right]}, \tag{2}$$

where η_x and η_y determine the relative weight assigned to the surrounding observation points. Larger values of η tend to smooth over small-scale variability in the parameter surface. As η approaches 0, the effect of small-scale variability is increased, while areas farther away from observations approach the population mean. The best fit model parameters are found simultaneously by nonlinear least squares fitting of the combined equations (1) and (2). We allow β to vary spatially by applying the model independently to data subsamples within a search radius ω.

[11] For independent variables we select physical and climate parameters that have been previously demonstrated to show high spatial correlation to SWE at the scale of the interpolation grid ($\sim$2 km) [*Carroll and Cressie*, 1997; *Fassnacht et al.*, 2003]. Here we use the three-dimensional position, slope, east aspect, north aspect, winter mean temperature, and total winter precipitation. Climate variables are adjusted to the SWE measurement elevation from the PRISM grid position using a lapse rate fitted to a nearest neighbor subsample of the data.

[12] Following a methodology similar to that of *Fassnacht et al.* [2003], each independent variable is ranked by the strength of spatial correlation between the variable and the set of observations. Each variable of successively lower correlation is included in the model so that each variable is tested but is discarded if model fit is not significantly improved. We extend this method by also testing higher orders ($1 \ldots p$) of the set of independent variables ($1 \ldots n$) again until the improvement in model fit is small or until the parameter matrix becomes rank deficient. The overall fit of each model is assessed through cross-validation root-mean-square error

$$\mathrm{RMSE}_m = \sqrt{\frac{1}{N} \sum_{i=1}^{n} \left[\hat{\mathrm{SWE}}_{i,m} - \mathrm{SWE}_i \right]^2}, \tag{3}$$

where, for each test model m, $\hat{\mathrm{SWE}}$ is predicted for the location of each ith observation using the other N-1 observations and is compared to the observed value SWE.

[13] For each parameter model X_m tested, the optimal regression radius ω is determined by a simplex search [*Nelder and Mead*, 1965]. The range of possible ω is confined by the number of stations needed in each regression to maintain a rank-sufficient parameter matrix. The optimal model and ω for each 1 April data set is then used to calculate $\hat{\mathrm{SWE}}$ at each point on the interpolation grid from the corresponding fields of independent variables. The 95% (1.96σ) confidence interval of $\hat{\mathrm{SWE}}$ at each observation point is determined from the variance in β, as given by the residuals and Jacobian of the nonlinear least squares solution.

3.2. Temporal Sensitivity Model

[14] The objective of temporal analysis is to constrain a sensitivity term relating variance in snow-water equivalent to corresponding temperature and precipitation at each grid cell. For this we assume that 1 April SWE varies with mean winter climate as

$$\begin{aligned} \mathrm{SWE} &= P + \alpha T, \quad T > T_{\min} \\ \mathrm{SWE} &= P, \quad T \le T_{\min}, \end{aligned} \tag{4}$$

where P and T are gridded winter total precipitation and average temperature, respectively. The climate sensitivity parameter α is analogous to a degree day constant in index melt models [*Hock*, 2003] and relates variance in SWE to variance in temperature forcing. Below a threshold temperature $T_{\min}$, SWE varies only with P. We estimate α for each grid cell by linear regression between the corresponding time series of $\hat{\mathrm{SWE}}$ and PRISM temperature and precipitation. We then obtain $T_{\min}$ from the value of T at $\mathrm{SWE} - P = 0$. In order to determine the confidence level of each α and $T_{\min}$ the regression is performed for a large number (500) of synthetic SWE time series drawn normal randomly from the variance of each $\hat{\mathrm{SWE}}$ estimate. Assuming a one-tailed normal distribution, the 95% confidence level is then constrained from the populations of α and $T_{\min}$ generated with the synthetic SWE data.

[15] Once the best fit α and uncertainty are determined for each grid cell, we then use the range of possible α and a prescribed change in P to integrate equation (4) over a range of temperature change. This yields the predicted change in snow-water equivalent volume $\hat{\mathrm{SWE}}^3$ as a function of the potential change in T and P.

4. Results

4.1. Spatial Model Error and Confidence

[16] The most often selected independent variables for the regression model were elevation, used for all years, and precipitation, used in 52 out of 53 years. Cross-validation errors for the interpolation models range from 7 to 36 cm, or 18 to 48% of that year's average SWE (Figure 2). Over the entire time series, there is a mean error of 18 cm, or 27% of the 53 year average, with no temporal trend in error. On average, the models were able to account for 68% of the spatial variance in measured SWE, reaching over 80%. The magnitude of error increases linearly with observed SWE, indicating an increasing degree of spatial variability with larger snowpack, although relative error decreases with greater snowpack. There is no clear relation between model error and which or how many independent variables were used in each annual model.

[17] The 95% confidence interval in $\hat{\mathrm{SWE}}$ averages 10–20% of the predicted value, with the largest uncertainties in the extreme northern end of the Sierra Nevada (Figure 3) due to poor regression fits. Estimate uncertainty closely follows the density of observations, with uncertainties

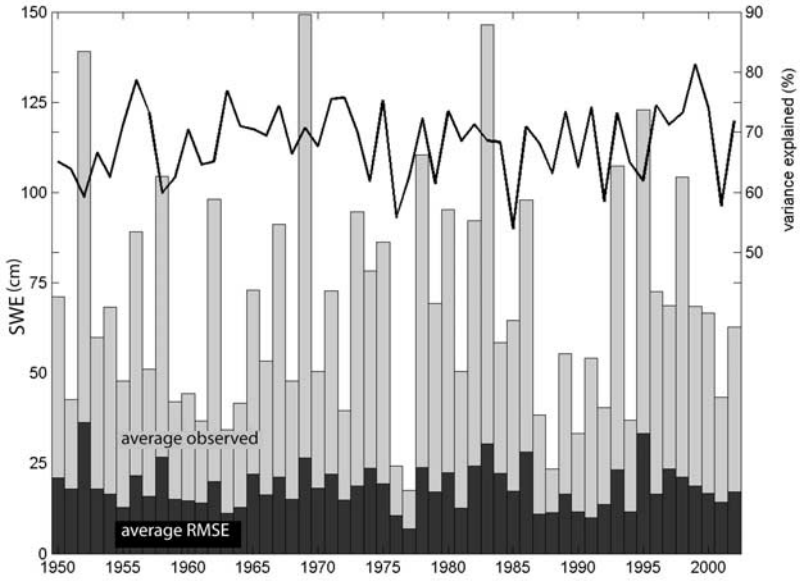

Figure 2. Time series of average 1 April Sierra Nevada snow-water equivalent (SWE) measured at 177 snow courses from 1950 to 2002 (gray bars) and average of cross-validation error (equation (3)) of the interpolation models (black bars). The line shows the percent of spatial variance in observed SWE explained by the best fit regression (right-hand scale).

reaching a minimum where observations are the most closely spaced between 2600 and 3200 m above sea level (masl) (Figure 4). On the basis of mean SWE, there is a bias in the distribution of stations toward the upper-middle end of the elevation range. Because of this bias, uncertainties reach over 100% below 1500 masl.

[18] Anomalously high uncertainties occurred during the winters of 1992–1993, 1995–1996, and 1997–1998, which were the only seasons with greater than 50% $\hat{SWE}^3$ estimate uncertainty. This is due to abnormally high local variability in snow course measurements, with stations recording up to 200% of normal in close proximity to stations registering near or below normal SWE. This results in poor model fitting and larger confidence intervals. It is unclear from the available data why these years would have such highly variable SWE, as there is no large abnormality in the spatial variance of precipitation or temperature.

4.2. Temporal Variations

[19] The 53 year time series of $\hat{SWE}^3$ shows large interannual fluctuations, with a standard deviation of approximately 50% of the 53 year mean and a weak

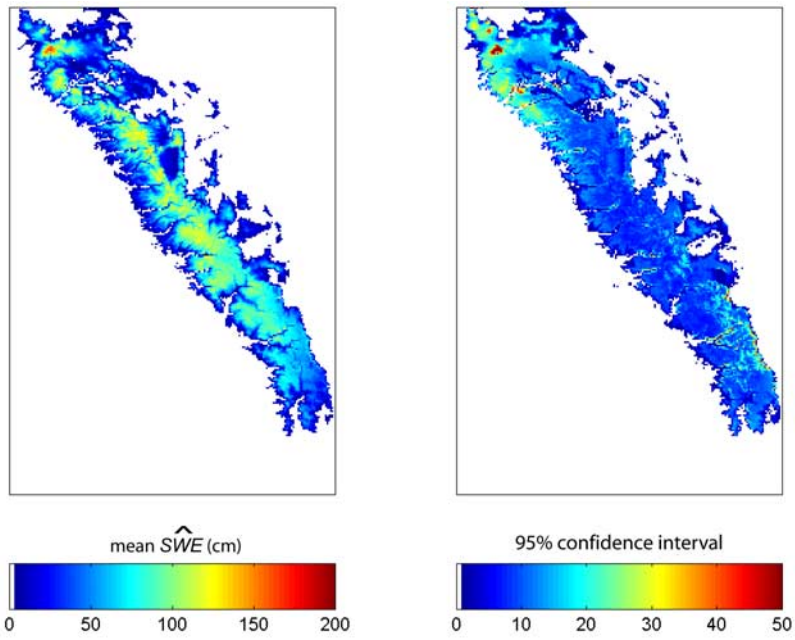

Figure 3. Maps of (left) modeled 1 April $\hat{SWE}$ for the period 1950–2002 interpolated from annual snow course observations and (right) the 95% (1.96σ) confidence interval of the predictions.

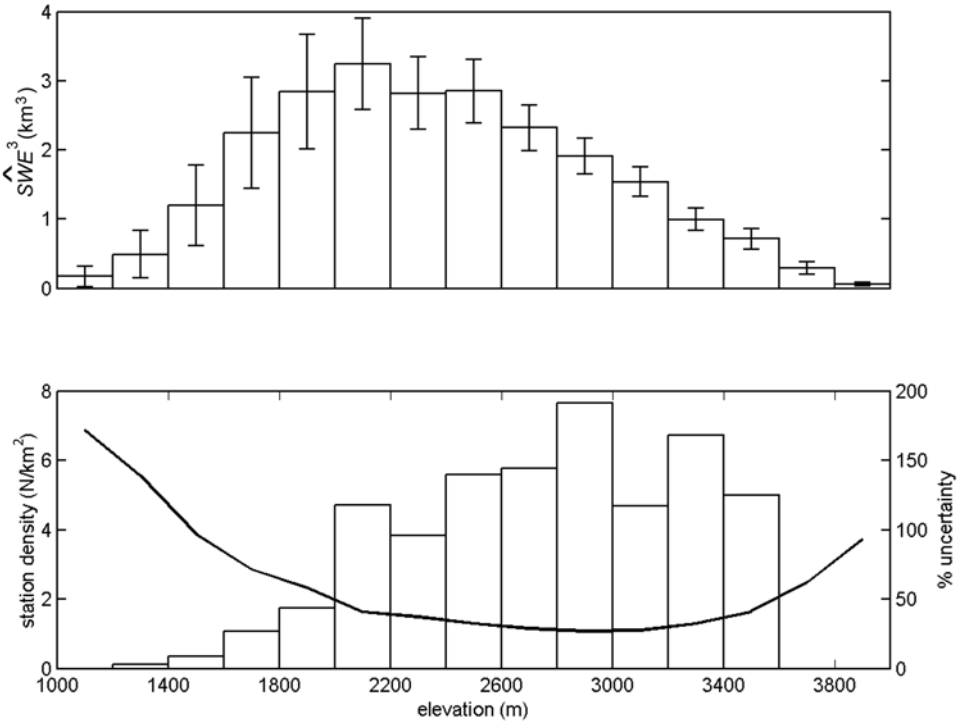

Figure 4. Histograms of (top) mean modeled $S\hat{W}E^3$ and (bottom) station density by elevation. Error bars show the range of mean uncertainty in volume estimates, also shown as a percent of $S\hat{W}E^3$ in Figure 4 (bottom, scale on the right-hand side). Station distribution is biased toward the higher elevations and does not agree with SWE distribution. This results in a sharp increase in relative prediction uncertainties below 2000 m above sea level (masl).

negative trend totaling 8% over the record (Figure 5). Separating the output by elevation, below 2500 masl the negative trend in $S\hat{W}E^3$ strengthens to 20%. Above 2500 masl, $S\hat{W}E^3$ has increased 15%. Considering the range as whole, this volume increase equals 40% of the volume loss below 2500 masl.

[20] Winter precipitation volume accounts for over 70% of the variance in $S\hat{W}E^3$ and has increased approximately 8%. Temperature accounts for 13% of the variance in $S\hat{W}E^3$ ($p = 0.01$) and shows a strong positive trend (>95% Mann's T confidence) of approximately 1°C over the time period. Below 2500 masl, temperature accounts for 23% of the variability in $S\hat{W}E^3$, while precipitation explains 55%. Above 2500 masl, P accounts for 91% of the variance in $S\hat{W}E^3$ and has increased by 9%. Winter temperature shows the strongest increase at higher altitudes at ~1.2°C but shows little or no correlation with $S\hat{W}E^3$.

4.3. Climate Sensitivity

[21] Values for α range from 0 to −20 cm °C^{-1}, with lowest (closest to zero) sensitivities occurring at elevations greater than 3200 m in the south (Figure 6). While α appears to be dependent on elevation in the southern half of the region, areas of high sensitivity occur at high elevations in the north, with the greatest sensitivity occurring in the areas around the Feather, American, and Yuba river drainages. Uncertainty in α averages 20% of the predicted values and corresponds to uncertainty in $S\hat{W}E$ (Figure 6), with uncertainty reaching over 100% of the predicted value in the extreme north and at the lowest elevations.

[22] Integrations of equation (4) were performed for changes in P of 0, 5, and −5% °C^{-1} (Figure 7). We limit application of the climate sensitivity model to a temperature change (δT) up to 5°C because the solution for α becomes less valid outside the temporal standard deviation of the T data. The decrease in land area with elevation results in slightly nonlinear loss in $S\hat{W}E^3$ with increasing temperature. In the $\delta P = 0$ case, there is a 6–10% decrease in $S\hat{W}E^3$ for each 1°C increase in winter temperature. For the δP = −5% °C^{-1} case the rate of change in $S\hat{W}E^3$ increases to −8 to −13% °C^{-1}, while for the P = +5% °C^{-1} case the rate of change in $S\hat{W}E^3$ decreases to −2 to −5% °C^{-1}. Increasing the rate of change of P to 8–12% °C^{-1} would result in no change in $S\hat{W}E^3$ up to $\delta T = 5$°C, with higher rates resulting in increasing $S\hat{W}E^3$. For this temperature range a 100% loss in $S\hat{W}E^3$ would require a 100% loss in P since T would still be less than T_{min} at the highest elevations.

4.4. Watershed Sensitivity

[23] Estimated $S\hat{W}E^3$ within 17 major Sierra Nevada watersheds accounts for an average of 76% of the variance in total summer unimpacted flow (Table 1). In general, this covariance is greater for higher-elevation watersheds. On average, total summer discharges are 70% of the watershed $S\hat{W}E^3$, which is a typical value for the ratio of runoff to snowmelt [*Viessman and Lewis*, 2002]. The high temporal correlation and reasonable relative values for summer discharge and $S\hat{W}E^3$ support the validity of the interpolation model estimates.

[24] Assessing climate sensitivity by watershed, we find that the lower-elevation drainages in the northwestern sector

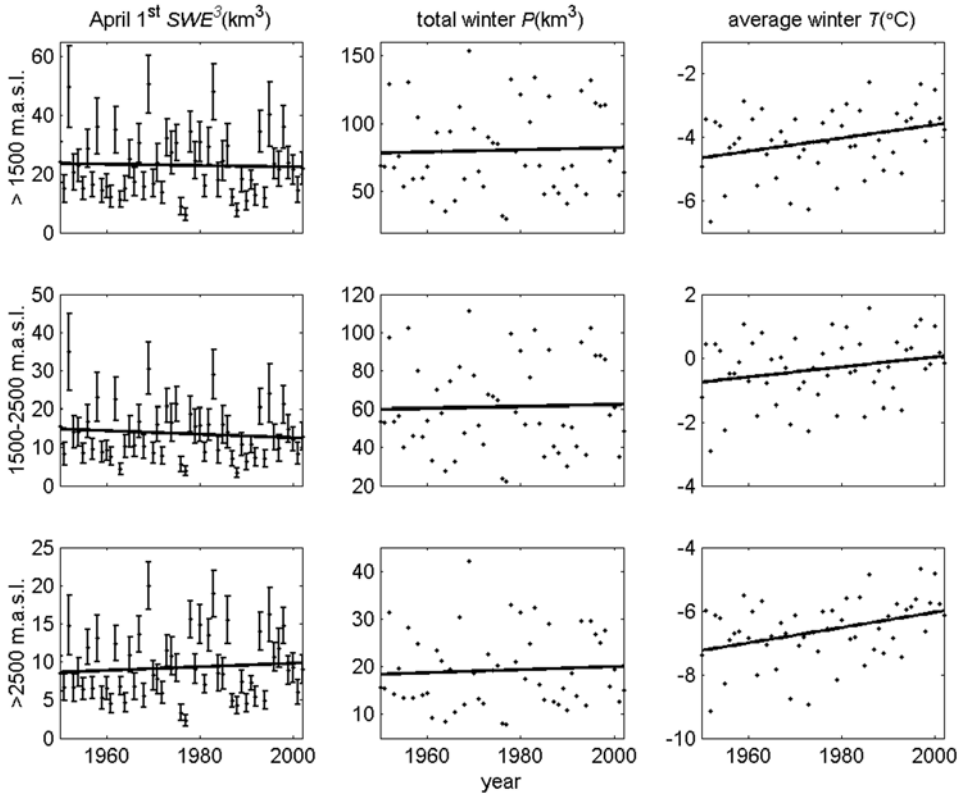

Figure 5. Time series and linear best fits of (left) $\hat{SWE}^3$, (middle) total winter (November–March) precipitation volume, and (right) mean winter temperature over the interpolation domain for elevations above 1500 masl, from 1500 to 2500 masl, and above 2500 masl. Error bars for $\hat{SWE}^3$ are the 95% confidence intervals.

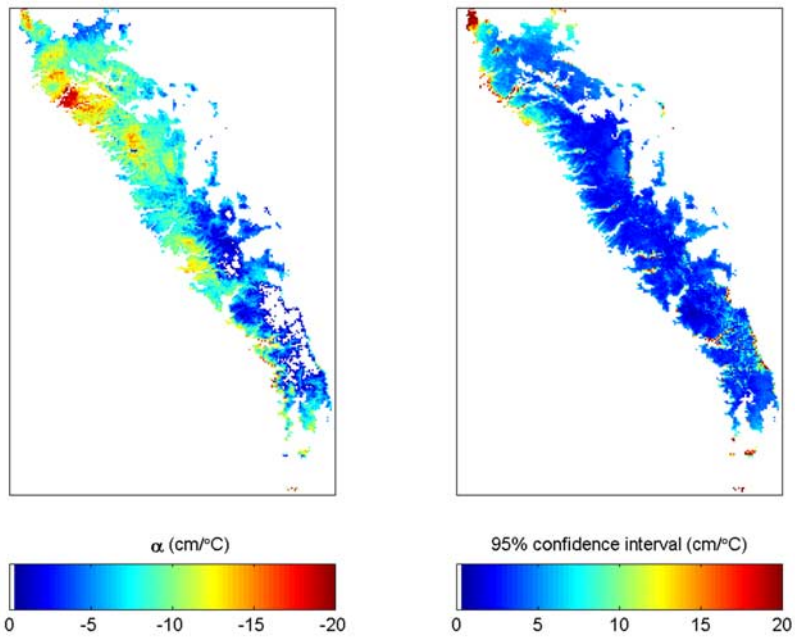

Figure 6. Maps of (left) climate sensitivity parameter values (α) and (right) confidence intervals obtained from least squares fitting of equation (4).

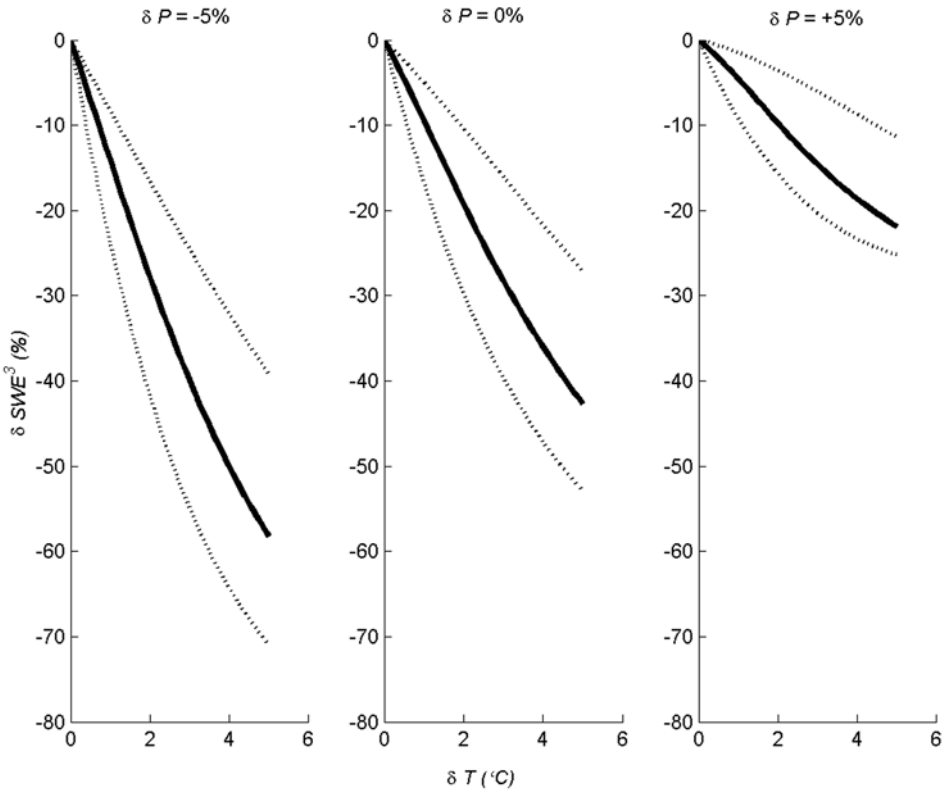

Figure 7. Change in SWE^3 as a percentage of the 1950–2002 mean versus change in mean winter temperature (δT) estimated from integration of equation (4) at each model grid cell using α and prescribed rates of change in winter precipitation (δP). Dotted lines are the estimate uncertainties (1.96σ) derived from the combined uncertainty in $\hat{SWE}^3$ and α.

of the study area, with the exception of the Tule basin in the south, would have the largest percent reduction in snow water volume under climate warming. The largest Sierra Nevada river by summer discharge, the Feather, is the most sensitive, losing from 17–28% of its total summer volume under a mean winter warming of 1°C up to 65% under 3°C warming. The San Joaquin, which drains the high southern Sierra, is the least sensitive, with a predicted loss of 22% under 3°C warming.

5. Discussion and Conclusions

[25] Total winter precipitation is the dominant control on both the spatial distribution and interannual variation in Sierra Nevada 1 April SWE, accounting for up to 90% of the spatial variance and over 50% of the temporal variation at even the lowest elevations. Therefore the high-resolution PRISM precipitation maps were essential for achieving model cross-validation errors much lower than interpolation schemes where only terrain variables were used [*Balk and Elder*, 2000; *Erxleben et al.*, 2002; *Fassnacht et al.*, 2003]. However, the dependence on precipitation may be over-predicted at low elevations because of the upper elevation bias in the observations (Figure 4). The greatest estimate uncertainties are in the northern Sierras because of the higher degree of spatial variability in SWE.

[26] The regional dependence of SWE on precipitation relative to temperature has resulted in little or no significant trend in 1 April $\hat{SWE}^3$ over the past half century despite a significant increase in mean winter temperatures. Increased melt at lower elevations from this warming has been significantly offset by an increase in precipitation, leading to an increase in $\hat{SWE}^3$ at higher elevations. Furthermore,

Table 1. Total Summer Discharge (Q) and Mean Elevation of Major Sierra Nevada Watersheds With Correlation (r^2) to Estimated 1 April Watershed Snow-Water Equivalent Volume ($\hat{SWE}^3$) and the 95% Confidence Interval of the Predicted Change in Watershed $\hat{SWE}^3$ (as a Percent of the 1950–2002 Mean) for Increases in Mean Winter Temperature Using the Climate Sensitivity Parameter

				$\delta\hat{SWE}^3$, %		
Drainage	Q, km^3	Altitude, masl	r^2	+1°C	+2°C	+3°C
American	1.6	1353	0.77	−11/−17	−23/−33	−34/−47
Carson	0.3	2233	0.81	−6/−11	−11/−21	−16/−31
Cosumnes	0.2	859	0.55	−14/−22	−27/−40	−40/−53
Feather	2.5	1560	0.70	−17/−28	−33/−49	−47/−65
Kaweah	0.4	1271	0.74	−8/−15	−16/−28	−22/−37
Kern	0.6	1818	0.83	−8/−17	−16/−31	−22/−41
Kings	1.6	2352	0.86	−4/−9	−8/−17	−11/−24
Merced	0.8	1706	0.84	−7/−12	−15/−23	−22/−33
Mokelumne	0.6	1247	0.82	−7/−12	−15/−24	−22/−35
Owens	0.1	2086	0.60	−3/−12	−6/−22	−9/−29
San Joaquin	1.6	2174	0.85	−4/−8	−9/−15	−13/−22
Stanislaus	0.9	1646	0.82	−8/−12	−16/−24	−23/−35
Truckee	0.3	2016	0.76	−13/−18	−26/−35	−38/−49
Tule	0.1	1243	0.58	−14/−24	−26/−41	−35/−52
Tuolumne	1.6	1857	0.85	−7/−11	−14/−21	−20/−30
Walker	0.3	2391	0.76	−4/−11	−7/−20	−11/−28
Yuba	1.3	1350	0.72	−12/−18	−23/−33	−34/−47

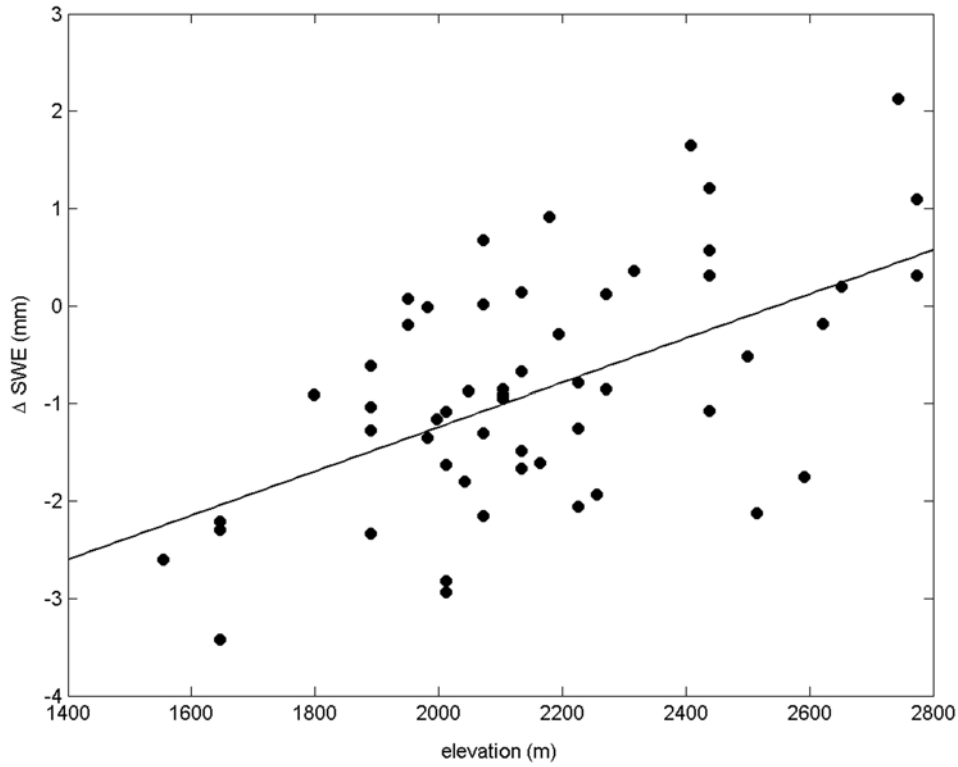

Figure 8. Elevation versus the trend in values for 1 April minus 1 March SWE for the period 1950–2002 for the 55 stations where records for both months exist. The best fit line has an r^2 of 0.3.

there has been no clear increase in the overall correlation between $\hat{SWE}^3$ and temperature, as would be expected under a strong warming trend. This pattern is markedly different from that of the Cascades to the north, where a similar warming trend and a decrease in precipitation has led to a widespread, significant loss of 1 April SWE [*Howat and Tulaczyk*, 2005; *Mote*, 2003; *Mote et al.*, 2005].

[27] The high interannual variability of winter climate in the Sierra Nevada region allows for prediction of the sensitivity parameter within a narrow confidence interval over the range of climate changes predicted by physical models for the near future (50–100 years from present). On the basis of past variance in SWE, spring snowpack at elevations below 2000 masl, as well as in the northern portion of the study area, is highly sensitive to temperature changes. While the elevation dependence of climate sensitivity is expected [*Kim*, 2001], the cause for the latitudinal dependence is unknown but may be due to a contrast in regional atmospheric patterns [*Knowles and Cayan*, 2002]. Higher elevations and much of the southern Sierra Nevada show very little sensitivity to temperature. Here a several degree increase in mean winter temperatures may result in only a 10–20% loss in $\hat{SWE}^3$.

[28] Since low-elevation snowpack is more sensitive to temperature, the difference between 1 April and 1 March SWE should be decreasing under warming at lower elevations. In Figure 8 we plot the 53 year trends in the values of 1 April minus 1 March SWE for the 55 stations that have records for both months. The trends in themselves are not statistically significant (all but one have a p value >0.05 using Mann's T) and are not correlated with latitude. However, the magnitudes of trends are highly correlated with elevation ($r^2 = 0.3$), with the change in 1 April minus 1 March SWE becoming increasingly negative at lower elevations and positive at higher ones. This correlation agrees with our sensitivity analysis and is evidence that melting is occurring earlier at lower elevations. This earlier melt would partly offset the positive contribution of an increase in winter precipitation to the 1 April volume budget.

[29] There is a wide degree of variability in climate sensitivity between individual watersheds, with the large watersheds in northern Sierra Nevada being especially sensitive to warming relative to the higher-elevation basins to the south (Table 1). Exactly how changes in snowpack may affect the discharge of individual rivers should depend, to a large extent, on basin hydrogeology. However, on a regional scale, this pattern is consistent with watershed models [*Knowles and Cayan*, 2002], although the magnitudes of potential sensitivity are much less in this analysis. For the majority of watersheds, loss of $\hat{SWE}^3$ due to warming may be offset by an increase in snow precipitation within the range expected from theoretical studies of potential atmospheric moisture changes (up to 10% $°C^{-1}$) [*Trenberth et al.*, 2003].

[30] The data show a weaker overall sensitivity to temperature change than predicted by physically based forecasting models. According to the covariance model, a change of 3°C over the next century would force a 30% decrease in $\hat{SWE}^3$, as opposed to 60% or greater in numerical models [*Kim et al.*, 2002; *Knowles and Cayan*, 2002; *Snyder et al.*, 2002, 2004]. This discrepancy in predicted change in $\hat{SWE}^3$ may be partly due to the higher spatial resolution, and therefore more detailed topography,

used in this study (~2 km) relative to atmospheric and regional hydrologic models (>10 km). The smoothed topography of these models may tend to underrepresent change at higher elevations, leading to an overprediction of the sensitivity of the land surface to temperature changes [*Cline et al.*, 1998]. Furthermore, the contribution of any potential increase in high-elevation precipitation to the total spring snow budget may be decreased or not included.

[31] Our analysis of historical data indicates that the potential impact of warming on snow water volume is highly dependent on concurrent precipitation changes and watershed topography. Existing model estimates of changes in precipitation under greenhouse warming scenarios have a high uncertainty and low spatial resolution [*Coquard et al.*, 2004; *Maurer and Duffy*, 2005; *Snyder et al.*, 2002]. Predictions of potential snow water volume changes based on these forecasts should therefore carry a high uncertainty as well.

[32] **Acknowledgments.** This work was funded by grants from the UC Center for Water Resources and the STEPS Institute. The authors thank J. Dozier and one anonymous reviewer for their helpful comments.

References

Aguado, E. (1990), Elevational and latitudinal patterns of snow accumulation departures from normal in the Sierra Nevada, *Theor. Appl. Climatol.*, *42*, 177–185.

Balk, B., and K. Elder (2000), Combining binary decision tree and geostatistical methods to estimate snow distribution in a mountain watershed, *Water Resour. Res.*, *36*, 13–26.

Bohr, G. S., and E. Aguado (2001), Use of April 1 SWE measurements as estimates of peak seasonal snowpack and total cold-season precipitation, *Water Resour. Res.*, *37*, 51–60.

California Department of Water Resources (1998), California water plan update, *Bull. Calif. Dep. Water Resour.*, *160-98*.

California Energy Commission (2003), 2003 Integrated energy policy report: Climate change and California, 46 pp., *Rep. 100-03-019*, Calif. Energy Comm., Sacramento.

Carroll, S. S., and N. Cressie (1997), Spatial modeling of snow-water equivalent using covariances estimated from spatial and geomorphic attributes, *J. Hydrol.*, *190*, 42–59.

Cline, D., K. Elder, and R. Bales (1998), Scale effects in a distributed snow-water equivalence and snowmelt model for mountain basins, *Hydrol. Processes*, *12*, 1527–1536.

Coquard, J., P. B. Duffy, K. E. Taylor, and J. P. Iorio (2004), Present and future surface climate in the western USA as simulated by 15 global climate models, *Clim. Dyn.*, *23*, 455–472.

Daly, C., G. H. Taylor, W. P. Gibson, T. W. Parzybok, G. L. Johnson, and P. Pasteris (2000a), High-quality spatial climate data sets for the United States and beyond, *Trans. ASAE*, *43*, 1957–1962.

Daly, S. F., R. E. Davis, E. Ochs, and T. Pangburn (2000b), An approach to spatially distributed snow modelling of the Sacramento and San Joaquin basins, California, *Hydrol. Processes*, *14*, 3257–3271.

Erxleben, J., J. K. Elder, and R. E. Davis (2002), Comparison of spatial interpolation methods for estimating snow distribution in the Colorado Rocky Mountains, *Hydrol. Processes*, *16*, 3627–3649.

Fassnacht, S. R., K. A. Dressler, and R. C. Bales (2003), Snow-water equivalent interpolation for the Colorado River Basin from snow telemetry (SNOTEL) data, *Water Resour. Res.*, *39*(8), 1208, doi:10.1029/2002WR001512.

Hock, R. (2003), Temperature index melt modelling in mountain areas, *J. Hydrol.*, *282*, 104–115.

Howat, I. M., and S. M. Tulaczyk (2005), Trends in California's snow-water volume over a half century of climate warming, *Ann. Glaciol.*, in press.

Kim, J. (2001), A nested modeling study of elevation-dependent climate change signals in California induced by increased atmospheric CO_2, *Geophys. Res. Lett.*, *28*, 2951–2954.

Kim, J., T. Kim, R. W. Arritt, and N. L. Miller (2002), Impacts of increased atmospheric CO_2 on the hydroclimate of the western United States, *J. Clim.*, *15*, 1926–1942.

Knowles, N., and D. R. Cayan (2002), Potential effects of global warming on the Sacramento/San Joaquin watershed and the San Francisco estuary, *Geophys. Res. Lett.*, *29*(18), 1891, doi:10.1029/2001GL014339.

Marquinez, J., J. Lastra, and P. García (2003), Estimation models for precipitation in mountainous regions: The use of GIS and multivariate analysis, *J. Hydrol.*, *270*, 1–11.

Maurer, E. P., and P. B. Duffy (2005), Uncertainty in projections of streamflow changes due to climate change in California, *Geophys. Res. Lett.*, *32*, L03704, doi:10.1029/2004GL021462.

Miller, N. L., K. E. Bashford, and E. Strem (2003), Potential impacts of climate change on California hydrology, *J. Am. Water Resour. Assoc.*, *39*, 771–784.

Mote, P. W. (2003), Trends in snow-water equivalent in the Pacific Northwest and their climatic causes, *Geophys. Res. Lett.*, *30*(12), 1601, doi:10.1029/2003GL017258.

Mote, P. W., A. F. Hamlet, M. P. Clark, and D. P. Lettenmaier (2005), Declining mountain snowpack in western North America, *Bull. Am. Meteorol. Soc.*, *86*, 39–49.

Nelder, J. A., and R. Mead (1965), A simplex method for function minimization, *Comput. J.*, *7*, 308–312.

Roos, M. (2003), California's cooperative snow surveys program, paper presented at 49th Annual Meeting of Cooperators, Calif. Coop. Snow Surv. Program, Folsom, Calif.

Serreze, M. C., M. P. Clark, R. L. Armstrong, D. A. McGinnis, and R. S. Pulwarty (1999), Characteristics of the western United States snowpack from snowpack telemetry (SNOTEL) data, *Water Resour. Res.*, *35*, 2145–2160.

Shelton, M. L., and R. M. Fridirici (1997), Decadal changes of inflow to the Sacramento San Joaquin delta, California, *Phys. Geogr.*, *18*, 215–231.

Snyder, M. A., J. L. Bell, L. C. Sloan, P. B. Duffy, and B. Govindasamy (2002), Climate responses to a doubling of atmospheric carbon dioxide for a climatically vulnerable region, *Geophys. Res. Lett.*, *29*(11), 1514, doi:10.1029/2001GL014431.

Snyder, M. A., L. C. Sloan, and J. L. Bell (2004), Modeled regional climate change in the hydrologic regions of California: A CO_2 sensitivity study, *J. Am. Water Resour. Assoc.*, *40*, 591–601.

Trenberth, K. E., A. Dai, R. M. Rasmussen, and D. B. Parsons (2003), The changing character of precipitation, *Bull. Am. Meteorol. Soc.*, *84*, 1205–1217.

Viessman, W., and G. L. Lewis (2002), *Introduction to Hydrology*, 5th ed., 624 pp., Prentice-Hall, Upper Saddle River, N. J.

I. M. Howat and S. Tulaczyk, Department of Earth Sciences, University of California, Santa Cruz, 1156 High Street, Santa Cruz, CA 95064, USA. (ihowat@pmc.ucsc.edu)